Journal of the Korean Crystal Growth and Crystal Technology
Vol. 26, No. 5 (2016) 165-170
http://dx.doi.org/10.6111/JKCGCT.2016.26.5.165

p-ISSN 1225-1429
e-ISSN 2234-5078

Correlation between composition and structure of Pt_xNi_y alloy nanodendrites

Young-Woo Lee, Da-Hee-Kwak* and Kyung-Won Park*,†

Department of Engineering Science, University of Oxford, Oxford OX1 3PJ, United Kingdom
**Department of Chemical Engineering, Soongsil University, Seoul 06978, Korea*

(Received September 27, 2016)
(Revised October 6, 2016)
(Accepted October 7, 2016)

Abstract We have synthesized Pt_xNi_y alloy nanodendrites by a thermal decomposition method. The structure and composition of the as-prepared samples were characterized by field-emission transmission electron microscopy (FE-TEM), energy dispersive X-ray (EDX) spectroscopy, and X-ray diffraction (XRD). The growth mode of the Pt_xNi_y alloy samples synthesized as a function of an intended atomic fraction of Ni was likely to be strongly affected by and reduction (or oxidation) potentials and surface energy.

Key words PtNi, Alloy, Nanodendrite, Composition, Structure

1. Introduction

Metallic nanoparticles (NPs) have received extensive interests due to their particular electrochemical, photochemical, biochemical, and catalytic properties [1-5]. In particular, shape-controlled metallic NPs have been synthesized with 0-dimensional (cube, octahedron, truncated cube, and tetrahedron) [6-10], 1-dimensional (wire, rod, and tube) [11-13], 2-dimensional (plate and sheet), and 3-dimensional (star, flower, and dendrite) structures [14-17]. Among them, the dendritic and flower-like nanostructures for electrochemical energy conversion devices such as fuel cells and metal-air batteries have shown much enhanced electrocatalytic activity and stability [18]. The metallic nanostructures have significantly enhanced electrocatalytic reaction rates over those of bulk materials. According to Xia, Wang, and Yang's works, Pt-based catalysts with dendritic nanostructures have exhibited improved methanol electrooxidation and oxygen reduction reactions because of high-index facets such as {311}, {730}, and {830} and high surface areas of the dendritic structures [18-20].

A variety of metallic NPs have been successfully prepared by means of chemical, thermal, electrochemical, and photochemical reduction methods [21-24]. Among them, the thermal decomposition method is suitable for the preparation of pure and metallic alloy NPs with homogeneous size and shape due to a well-defined inverse micelle structure in organic based solutions [25-27]. Herein, we synthesized Pt-Ni alloy nanodendrites (Pt_xNi_y) with various elemental compositions using thermal-decomposition method. The Pt_xNi_y alloy nanodendrites were prepared by simultaneously reducing platinum acetylacetonate and nickel acetylacetonate in 1-octadecene as solvent, oleylamine, and oxalic acid at 250°C for 2 h. The long-alkane-chain amine such as oleylamine was used as a main capping agent, which is important in determining the shape and distribution of the nanoparticles. The structure and composition of the Pt-Ni alloy nanodendrites were characterized by field-emission transmission electron microscopy (FE-TEM), energy dispersive X-ray (EDX) spectroscopy, and X-ray diffraction (XRD).

2. Experiments

The Pt-Ni alloy nanodendrites were prepared by reducing Pt and Ni salt in organic-based solution. All chemicals used were of analytical grade. The metal salts for the Pt-Ni alloy NPs were dissolved in 5 mL 1-octadecene ($C_{18}H_{36}$, Aldrich) and 4.22 mL oelyamine ($C_{18}H_{37}N$, Aldrich) solution as the following ratios: 4.8 mM platinum acetylacetonate ($Pt(acac)_2$, Aldrich) and 1.2 mM nickel acetylacetonate ($Ni(acac)_2$, Aldrich) for Pt_4Ni_1 NPs, 4.5 mM $Pt(acac)_2$ and 1.5 mM $Ni(acac)_2$ for Pt_3Ni_1 NPs, 4.0 mM $Pt(acac)_2$ and 2.0 mM $Ni(acac)_2$ for Pt_2Ni_1 NPs, 3.0 mM $Pt(acac)_2$ and 3.0 mM $Ni(acac)_2$ for Pt_1Ni_1 NPs, 2.0 mM $Pt(acac)_2$ and 4.0 mM $Ni(acac)_2$ for Pt_1Ni_2 NPs, 1.5 mM $Pt(acac)_2$ and 4.5 mM $Ni(acac)_2$ for Pt_1Ni_3 NPs, and 1.2 mM $Pt(acac)_2$ and 4.8 mM $Ni(acac)_2$ for

†Corresponding author
E-mail: kwpark@ssu.ac.kr

Pt_1Ni_4 NPs. For the complete dissolution of metal salts, the metal salt solutions were kept with continuous stirring for 30 min at 70°C. On the other hand, the mixture solution of 10.78 mL 1-octadecene and 5 mL oleylamine containing 50.4 mg oxalic acid ($C_2H_2O_4 \cdot 2H_2O$, Johnson Matthey Co.) was prepared in a three-neck flask under a nitrogen atmosphere. The mixture solution was raised by 7°C min^{-1} and kept for 2 h at 250°C. The metal salt solutions were injected into the mixture solution with continuous stirring and kept for 2 h at 250°C until the metal salts were completely reduced into metallic nanostructures under nitrogen atmosphere. The resulting black colloid solutions were rapidly cooled into hexane indicating the formation of Pt-Ni alloy NPs.

The structure and chemical composition of the samples were characterized using FE-TEM (Philips Tecnai F20 system operating at 200 kV) and energy dispersive X-ray (EDX) spectroscopy. XRD analysis (Bruker D2 Phase system equipped with a Cu K_α radiation source of $\lambda = 0.15406$ nm and a Ni filter) was performed to confirm the crystal structure of the as-prepared samples.

3. Results and Discussion

The structure analysis of the as-synthesized Pt_xNi_y NPs was examined by FE-TEM. The Pt_xNi_y NPs exhibit dendritic nanostructures as indicated in Fig. 1. The average sizes of Pt_4Ni_1, Pt_3Ni_1, Pt_2Ni_1, Pt_1Ni_1, Pt_1Ni_2, Pt_1Ni_3, and Pt_1Ni_4 NPs are ~27.7, ~21.7, ~31.4, ~40.8, ~38.2, ~32.1, and ~36.2 nm, respectively. As confirmed by EDX profiles, the elemental compositions of Pt and Ni in the dendritic NPs are 82 and 18 at% for Pt_4Ni_1, 75 and 25 at% for Pt_3Ni_1, 70 and 30 at% for Pt_2Ni_1, 55 and 45 at% for Pt_1Ni_1, 60 and 40 at% for Pt_1Ni_2, 52 and 48 at% for Pt_1Ni_3, and 60 and 40 at% for Pt_1Ni_4, respectively, (Fig. 1(c), (f), (i), (l), (o), (r), and (u)), indicating the restricted Ni reduction in the present synthetic atmosphere. As observed by energy dispersive X-ray (EDX) spectra, the as-prepared Pt_xNi_y NPs show homogenous

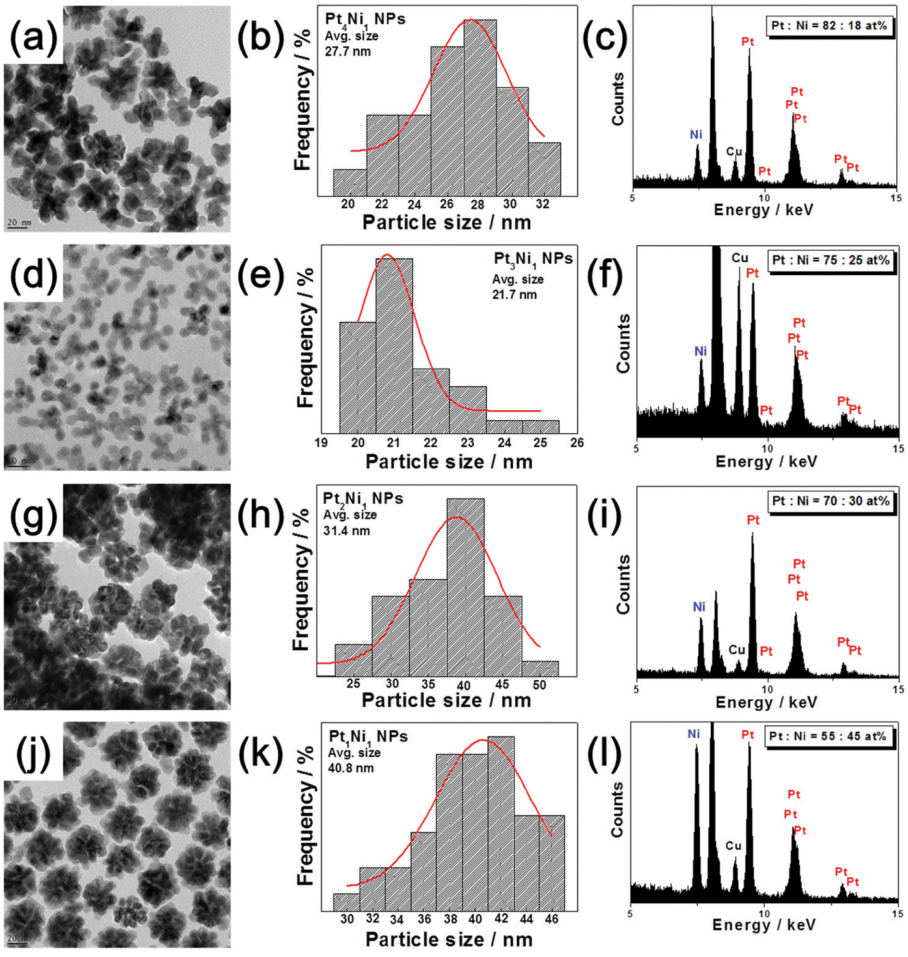

Fig. 1. TEM images ((a), (d), (g), (j), (m), (p), and (s)), particle size histograms ((b), (e), (h), (k), (n), (q), and (t)), and EDX spectra ((c), (f), (i), (l), (o), (r), and (u)) for Pt_4Ni_1, Pt_3Ni_1, Pt_2Ni_1, Pt_1Ni_1, Pt_1Ni_2, Pt_1Ni_3, and Pt_1Ni_4 alloy NPs, respectively.

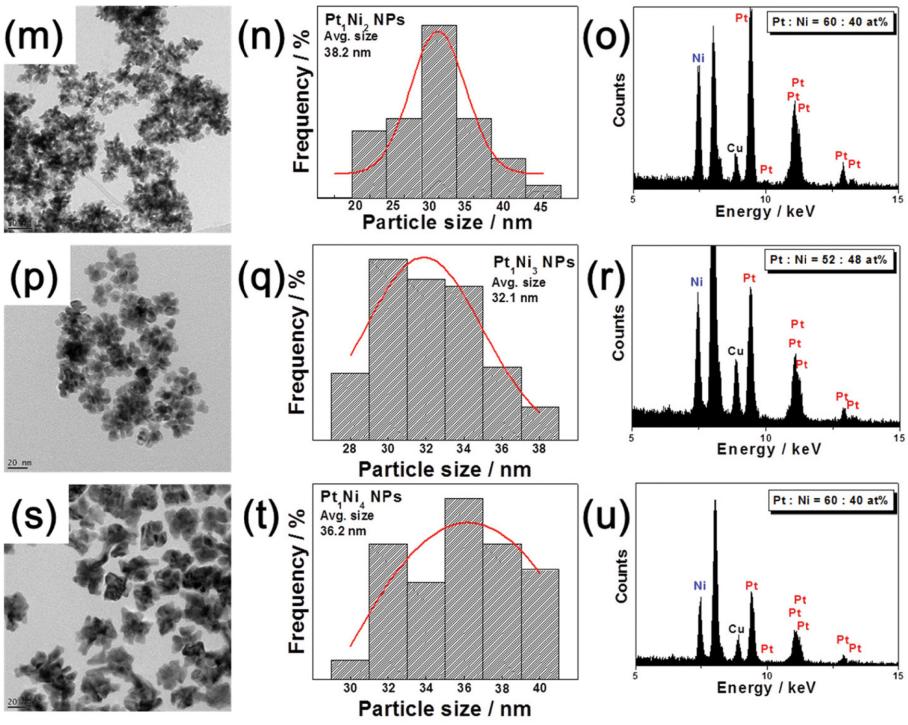

Fig. 1. Continued.

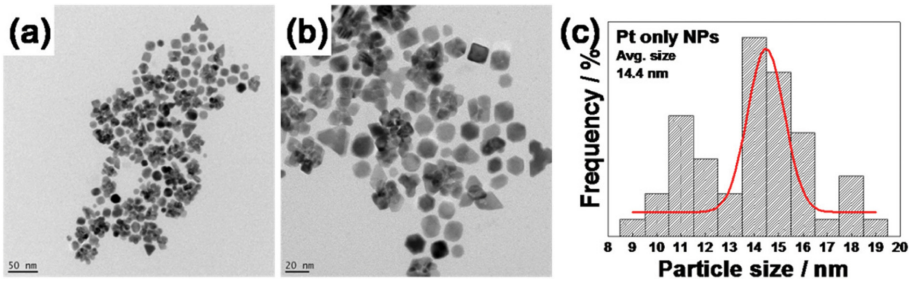

Fig. 2. (a) and (b) TEM images and (c) particle size histogram of pure Pt NPs.

distributions of both platinum and nickel in the dendritic shape. On the other hand, in the absence of $Ni(acac)_2$, the Pt NPs exhibit polygonal shapes such as octahedron, cube, and cuboctahedron (Fig. 2).

Fig. 3(a) shows XRD patterns of pure Pt, Pt_4Ni_1, Pt_3Ni_1, and Pt_1Ni_1 NPs. Assuming a substitutional solid solution between metallic phases, higher angle shift of the XRD peaks indicates alloy formation between Pt and Ni. The XRD peaks in the Pt_xNi_y NPs are shifted into higher 2θ values with increasing amount of Ni in (220) diffraction peaks. The lattice parameters of the Pt_xNi_y NPs are given in Fig. 3(b), reflecting the degree of alloying in the bimetallic structures. Since the radius of Pt atom (0.139 nm) is greater than the radius of Ni atom (0.125 nm), the crystalline lattice parameters of the Pt_xNi_y NPs decrease with decreasing elemental composition of Pt as summarized in Table 1. Until the intended Pt atomic fraction decreases to 50 at%, the Pt_xNi_y NPs appear on a straight fitted line based on the solid solution between Pt and Ni, which means a well-defined alloy formation between Pt and Ni in Fig. 3(b). On the other hand, as the intended atomic fraction of Pt is less than 50 at%, the Pt_xNi_y alloy NPs exhibit almost no angle shift of the XRD peaks, in agreement with lattice parameter of Pt_1N_1. The elemental Pt and Ni containing in the Pt_xNi_y NPs are believed to be alloyed by combining EDX and XRD results.

Fig. 4 shows a plot of atomic fraction of Ni and average particle size of the as-synthesized Pt_xNi_y alloy NPs as a function of an intended atomic fraction of Ni. Until the intended Ni atomic fraction increases to 50 at%, both the measured atomic fraction of Ni and average particle size of the Pt_xNi_y alloy NPs increase. However, as the intended atomic fraction of Ni is more than 50

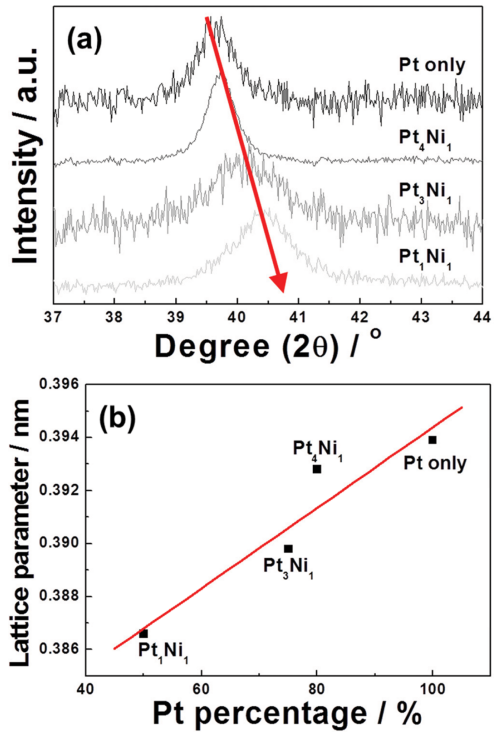

Fig. 3. (a) XRD peaks of (220) planes in the Pt_xNi_y NPs compared with XRD reference data. (b) Plot of lattice parameter *versus* Pt atomic percentage of the Pt_xNi_y NPs.

Table 1
Comparison of the lattice parameter between Pt_xNi_y alloy NPs

Samples	2θ	a/nm
Pure Pt	39.63	0.3939
Pt_4Ni_1	39.74	0.3928
Pt_3Ni_1	40.06	0.3898
Pt_1Ni_1	40.41	0.3866
Pure Ni	44.546	0.3523

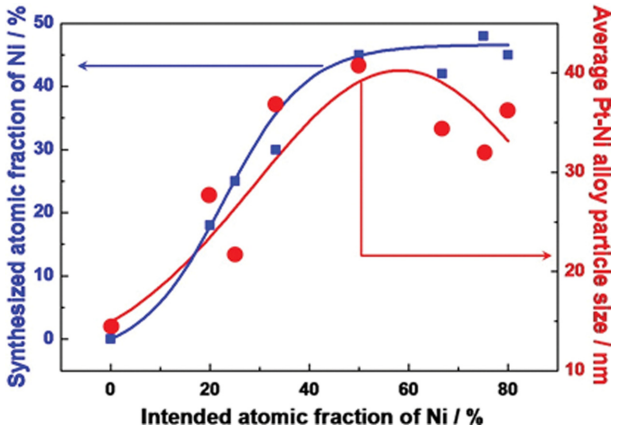

Fig. 4. Plot of the measured atomic fraction of Ni and average particle size of the Pt_xNi_y alloy NPs as a function of the intended atomic fraction of Ni.

at%, the measured Ni atomic fraction is saturated and average particle size of the Pt_xNi_y alloy NPs slightly decreases. Fig. 5 shows HR-TEM images and FFT patterns of the Pt_xNi_y alloy NPs synthesized with different intended ratios of Ni. Until the intended ratio of Ni increases to 50 at%, the as-synthesized Pt_xNi_y alloy NPs

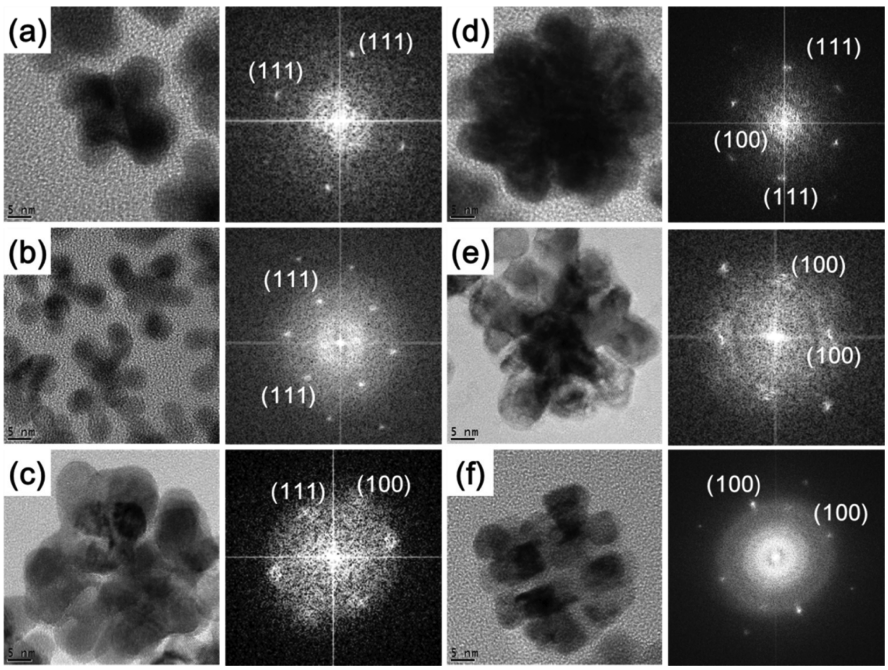

Fig. 5. HR-TEM images and fast Fourier-transform (FFT) patterns of (a) Pt_4Ni_1, (b) Pt_3Ni_1, (c) Pt_2Ni_1, (d) Pt_1Ni_1, (e) Pt_1Ni_2, and (f) Pt_1Ni_3 alloy NPs.

exhibit fairly round pod-shape nanostructures with majority {111} facets and minority {100} facets. However, as the intended atomic fraction of Ni is more than 50 at%, the as-synthesized Pt_xNi_y alloy NPs exhibit fairly angular pod-shape nanostructures with dominant {100} facets.

Considering the growth mechanism of the Pt_xNi_y alloy NPs with different intended ratios of Ni, two feasible factors to determine a transition of the Pt_xNi_y alloy NPs are likely to be as follows: a) oxidation and reduction potentials of Ni species and b) surface energies of low-index facets in metallic phases such as Pt and Ni. Firstly, according to the potential effect, standard oxidation and reduction potentials of Ni species are as follows:

$$Ni^{2+} + 2e^- \rightarrow Ni^0 \qquad E = -0.257\ V \qquad (1)$$

The reduction of nickel ions having a negative potential value in Equation (1) is not thermodynamically spontaneous. In contrast, the oxidation of metallic Ni into nickel ions occurs in the present reaction containing hydroxyl ion in oxalic acid. Thus, this means that although the intended atomic fraction of Ni is an excess of amount, the reduced amount of Ni salts and the size of as-prepared NPs can be limited under the same thermal energy. As already observed in Fig. 4, although the intended atomic fraction of Ni is more than 50 at%, both the reduced Ni atomic fraction and average particle size for the Pt_xNi_y alloy NPs are likely to be restricted due to the potential effect. Secondly, from the view point of surface energy of metallic phase such as Pt and Ni, the metallic NPs synthesized by fast reduction reaction such as a thermal decomposition process tend to thermodynamically minimize the surface energy of NPs thus forming crystal facets with the lower surface energy in the nanostructures. In the case of Pt, the surface energies of {111}, {100}, and {110} facets are 1.004, 1.378, and 2.009 eV $atom^{-1}$, respectively. On the other hand, the surface energies of {111}, {100}, and {110} facets in Ni are 0.695, 0.969, and 1.337 eV $atom^{-1}$, respectively. When the amount of Pt increases from $x = 2$ to from $x = 4$ in Pt_xNi_1, i.e. under Pt-rich synthetic atmosphere, the Pt_xNi_y alloy NPs exhibit dominant {111} facets (Fig. 3(a)~(c)). In contrast, when the amount of Ni increases from $y = 2$ to $y = 4$ in Pt_1Ni_y, i.e. under Ni-rich synthetic atmosphere, the Pt_xNi_y alloy NPs exhibit dominant {100} facets (Fig. 3(e) and (f)). Thus, it is concluded that the growth mode of the Pt_xNi_y alloy NPs is strongly affected by both reduction (or oxidation) potentials and surface energy.

4. Conclusions

We have synthesized Pt_xNi_y alloy nanodendrites by a thermal decomposition method. The as-synthesized Pt_xNi_y alloy catalyst exhibited 3-dimentional dendritic structure with fairly uniform particle size and shape. In particular, the growth mode of the Pt_xNi_y alloy NPs synthesized as a function of an intended atomic fraction of Ni is likely to be strongly affected by and reduction (or oxidation) potentials and surface energy.

Acknowledgments

This work was supported by the International Collaborative Energy Technology R&D Program of the Korea Institute of Energy Technology Evaluation and Planning (KETEP), granted financial resource from the Ministry of Trade, Industry & Energy, Republic of Korea (No. 20148520120160).

References

[1] I.-T. Kim, H.-K. Lee and J. Shim, "Synthesis and characterization of Pt-Pd catalysts for methanol oxidation and oxygen reduction", J. Nanosci. Nanotech. 8 (2008) 5302.
[2] S.-W. Xie, S. Chen, Z.-Q. Liu and C.-W. Xu, "Comparison of alcohol electrooxidation on Pt and Pd electrodes in alkaline medium", Int. J. Electrochem. Sci. 6 (2011) 882.
[3] S. Lj. Gojković, T.R. Vidaković and D.R. Durović, "Kinetic study of methanol oxidation on carbon-supported PtRu electrocatalysts", Electrochim. Acta 48 (2003) 3607.
[4] J.M.S. Ayub, R.F.B. De Souza, J.C.M. Silva, R.M. Piasentin, E.V. Spinacé, M.C. Santos and A.O. Neto, "Ethanol electro-oxidation on PtSn/C-ATO electrocatalysts", Int. J. Electrochem. Sci. 7 (2012) 11351.
[5] M.D. Obradović and S. Lj. Gojković, "Electrochemical instability of Pt nanoparticles probed by formic acid oxidation", J. Electroanal. Chem. 664 (2012) 152.
[6] Y.W. Lee, M. Kim and S.W. Han, "Shaping Pd nanocatalysts through the control of reaction sequence", Chem. Commun. 46 (2010) 1535.
[7] Y. Kang, X. Ye and C.B. Murray, "Size- and shape-selective synthesis of metal nanocrystals and nanowires using CO as a reducing agent", Angew. Chem. Int. Ed. 49 (2010) 6156.
[8] Y.-W. Lee, A-R. Ko, S.-B. Han, H.-S. Kim, D.-Y. Kim, S.-J. Kim and K.-W. Park, "Cuboctahedral Pd nanoparticles on WC for enhanced methanol electrooxidation in alkaline solution", Chem. Commun. 46 (2010) 9241.
[9] Y.-W. Lee, A-R. Ko, S.-B. Han, H.-S. Kim and K.-W. Park, "Synthesis of octahedral Pt-Pd alloy nanoparticles

for improved catalytic activity and stability in methanol electrooxidation", Phys. Chem. Chem. Phys. 13 (2011) 5569.
[10] Y.-W. Lee, S.-B. Han, A-R. Ko, H.-S. Kim and K.-W. Park, "Glycerol-mediated synthesis of Pd nanostructures with dominant {111} facets for enhanced electrocatalytic activity", Catal. Commun. 15 (2011) 137.
[11] D. Seo and H. Song, "Asymmetric hollow nanorod formation through a partial galvanic replacement reaction", J. Am. Chem. Soc. 131 (2009) 18210.
[12] L. Wang and Y. Yamauchi, "Autoprogrammed synthesis of triple-layered Au@Pd@Pt core-shell nanoparticles consisting of a Au@Pd bimetallic core and nanoporous Pt shell", J. Am. Chem. Soc. 132 (2010) 13636.
[13] Z. Chen, M. Waje, W. Li and Y. Yan, "Supportless Pt and PtPd nanotubes as electrocatalysts for oxygen-reduction reactions", Angew. Chem. Int. Ed. 46 (2007) 4060.
[14] A. Mohanty, N. Garg and R. Jin, "A universal approach to the synthesis of noble metal nanodendrites and their catalytic properties", Angew. Chem. Int. Ed. 49 (2010) 4962.
[15] B. Lim, M. Jiang, T. Yu, P.H.C. Camargo and Y. Xia, "Nucleation and growth mechanisms for Pd-Pt bimetallic nanodendrites and their electrocatalytic properties", Nano Res. 3 (2010) 69.
[16] L. Wang, Y. Nemoto and Y. Yamamuchi, "Direct synthesis of spatially-controlled Pt-on-Pd bimetallic nanodendrites with superior electrocatalytic activity", J. Am. Chem. Soc. 131 (2011) 9674.
[17] L. Wang and Y. Yamaumchi, "Block copolymer mediated synthesis of dendritic platinum nanoparticles", J. Am. Chem. Soc. 131 (2009) 9152.
[18] Z. Peng and H. Yang, "Synthesis and oxygen reduction electrocatalytic property of Pt-on-Pd baimetallic heteronanostructures", J. Am. Chem. Soc. 131 (2009) 7542.
[19] B. Lim, M. Jiang, P.H.C. Camargo, E.C. Cho, J. Tao, X. Lu and Y. Xia, "Pd-Pt bimetallic nanodendrites with high activity for oxygen reduction", Science 324 (2009) 1302.
[20] N. Tian, Z.-Y. Zhou, S.-G. Sun, Y. Ding and Z. L. Wang, "Synthesis of tetrahexahedral platinum nanocrystals with high-index facets and high electro-oxidation activity", Science 316 (2007) 732.
[21] S.-I. Choi, R. Choi, S.W. Han and J.T. Park, "Synthesis and characterization of Pt_9Co nanocubes with high activity for oxygen reduction", Chem. Commun. 46 (2010) 4950.
[22] Q. Zhang, J. Xie, J. Liang and J.Y. Lee, "Synthesis of monodisperse Ag-Au alloy nanoparticles with independently tunable morphology, composition, size, and surface chemistry and their 3-D superlattices", Adv. Funct. Mater. 19 (2009) 1387.
[23] H. Lee, S.E. Habas, S. Kweskin, D. Butcher, G.A. Somorjai and P. Yang, "Morphological control of catalytically active platinum nanocrystals", Angew. Chem. Int. Ed. 45 (2006) 7824.
[24] Y.-W. Lee, J.-K. Oh, H.-S. Kim, J.-K. Lee, S.-B. Han, W. Choi and K.-W. Park, "Shape-controlled Pd nanostructure catalysts for highly efficient electrochemical power sources", J. Power Sources 195 (2010) 5896.
[25] M. Subhramannia and V.K. Pillai, "Shape-dependent electrocatalytic activity of platinum nanostructures", J. Mater. Chem. 18 (2008) 5858.
[26] Y. Bing, H. Liu, L. Zhang, D. Ghosh and J. Zhang, "Nanostructured Pt-alloy electrocatalysts for PEM fuel cell oxygen reduction reaction", Chem. Soc. Rev. 39 (2010) 2184.
[27] Y.-W. Lee, S.-B. Han, D.-Y. Kim and K.-W. Park, "Monodispersed platinum nanocubes for enhanced electrocatalytic properties in alcohol electrooxidation", Chem. Commun. 47 (2011) 6296.